OPEN ACCESS

Effect of Hydrogen on the Dissolution of Uranium Dioxide in Peroxide-Containing Environments

Journal of The Electrochemical Society, 2023 **170** 096506

Effect of Hydrogen on the Dissolution of Uranium Dioxide in Peroxide-Containing Environments

Martin D. M. Badley,[1] David W. Shoesmith,[1,2] and James J. Noël[1,2,z]

[1]*Department of Chemistry, The University of Western Ontario, London, Ontario N6A 3K7, Canada*
[2]*Surface Science Western, The University of Western Ontario, London, Ontario N6G 0J3, Canada*

The ability of hydrogen (H_2) to scavenge hydroxy radicals ($OH^{\bullet}$) created by the dissociation of hydrogen peroxide (H_2O_2) on the surface of uranium dioxide ($U^{IV}O_2$) has been studied in a chloride/bicarbonate (pH = 9.5) solution. The oxidation/reduction of the oxide surface was monitored by measuring the corrosion potential as a function of time in this solution, containing various concentrations of H_2O_2 sparged with either Ar or an Ar/H_2 mixture. The surface oxidation was subsequently determined using X-ray photoelectron spectroscopy. In the absence of H_2, the peroxide oxidized the surface to $U^{IV}_{1-2x}U^{V}_{2x}O_{2+x}$ with x varying with H_2O_2 concentration and eventually achieved a composition of $U^{IV}_{0.34}U^{V}_{0.66}O_{2.33}$. At this surface composition, the surface becomes unstable with respect to dissolution, but the dominant reaction is H_2O_2 decomposition. In the presence of H_2, the initial oxidation of the $U^{IV}O_2$ when H_2O_2 was added was reversed by the ability of H_2 to scavenge the $OH^{\bullet}$ with the $H^{\bullet}$ radicals formed. This led to a reduction of the oxidized surface. The efficiency of this process is determined by the relative concentrations of H_2O_2 and H_2.
 [DOI: 10.1149/1945-7111/acf52b]

Manuscript submitted July 11, 2023; revised manuscript received August 17, 2023. Published September 20, 2023.

The internationally accepted approach for the disposal of high-level nuclear waste is to isolate and contain it within a deep geologic repository (DGR). Canada's design to ensure the containment of used nuclear fuel is to seal it in a corrosion-resistant Cu-coated steel container isolated within a multiple barrier system composed of the fuel waste form, the container, bentonite clay buffer and seals around the container and the surrounding host rock. While the container will provide long-term containment,[1] it is necessary to evaluate the potential consequences of its failure when the fuel waste form could come in contact with groundwater. An extensive international effort has been expended on determining fuel behaviour and the possible release from the fuel of radionuclides under a range of DGR conditions.[2–13]

The groundwater entering the breachedcontainer will be anoxic, the dissolved O_2 in the vicinity of the container having been consumed by reactions with organic matter, oxidizable minerals in the clay buffer and the host rock, and container corrosion processes. Consequently, the radiolysis of the groundwater will be the only source of oxidants within the container. Since U solubility increases by many orders of magnitude when U^{IV} is oxidized to U^{VI} (as UO_2^{2+}),[14] radiolytic oxidants, in particular, H_2O_2, will lead to fuel corrosion and radionuclide release.[15] However, the radiolysis of H_2O and the corrosion of the carbon steel container will produce the oxidant scavengers H_2 and Fe^{2+}, which will suppress oxidizing conditions at the UO_2 surface by both homogeneous and heterogeneous reactions.[16–18] Of these two potential reducing agents, H_2 has been shown to be dominant in suppressing corrosion.[16,17,19] Consequently, the influence of H_2 on fuel corrosion has been extensively studied as summarized by Badley and Shoesmith, and references therein.[13]

For dissolved H_2 to act as a reductant, it must be activated, i.e., dissociated into reactive $H^{\bullet}$ radicals. This has been shown to occur on the surfaces of simulated spent nuclear fuels (SIMFUEL), catalyzed by noble metal (ε) particles composed of metals known to catalyze H_2 dissociation [Rh, Pd, Ru, Mo].[20] These particles are galvanically coupled to the UO_2 matrix and act as anodes which catalyze $H^{\bullet}$ oxidation to H^+, forcing the matrix to adopt a corrosion potential (E_{CORR}) too low for the oxidation/dissolution of UO_2. In the absence of such particles, galvanic protection does not occur, with experiments indicating minimal activation of H_2 on the UO_2 surface.[19] Activation can also be achieved in the presence of radiation (both α and γ) with the radiolytically-produced $H^{\bullet}$ on the UO_2 surface acting as a scavenger for radiolytic oxidants, a process shown to suppress their reaction with UO_2.[19,21–28]

Since the noble metals in the ε-particles are catalytic for both the reduction of oxidants, such as H_2O_2, as well as the oxidation of H_2, it is not surprising that UO_2 oxidation in H_2O_2 solutions containing H_2 can be suppressed when noble metals are present either as particles in the UO_2 surface or as separated powder in the solution.[19,29–31] However, experiments in which H_2O_2 was added to Ar/H_2-sparged solutions in the presence of a SIMFUEL containing no ε-particles suggested, but did not clearly demonstrate, that H_2 scavenging could also occur directly on the UO_2 surface. This would not be surprising since H_2O_2 reactions (particularly its decomposition to O_2 and H_2O) have been shown to proceed via the formation of surface $OH^{\bullet}$ radicals, introducing the possibility that they could be scavenged by reactions with soluble H_2 on the UO_2 surface in the absence of radiation and ε-particles.[32–38]

In this study, the role of the UO_2 surface in reactions involving H_2O_2 and H_2 is investigated using a combination of electrochemical and surface analytical techniques.

Experimental

Electrode materials and preparation.—Experiments were conducted on an un-doped natural UO_2 electrode cut as a 2 mm-thick disc from a commercial fuel pellet manufactured by Zircatec Precision Industries (Now Cameco Fuel Manufacturing, Port Hope, Ontario) in September 1990. The details of electrode preparation have been discussed previously.[39] The surface area of the single exposed face of the disc was 1.16 cm^2. The resistivity of UO_2 is known to be sensitive to the degree of hyperstoichiometry (x in UO_{2+x}).[40–44] The measured resistance of the specimen used was 10 kΩ.cm. This is close to that measured on a $UO_{2.002}$ specimen,[45] suggesting the pellet may have had a slight residual excess O within the matrix. Before each experiment, the electrode was groundwith 1200 grit SiC paper, then sonicated for 2 min in Type 1 H_2O (resistivity = 18.2 MΩ.cm) to remove polishing debris.

Solution preparation.—Solutions were prepared using Type 1 H_2O from a Millipore Milli-Q direct water purification system and deaerated using either Ar or 5% H_2/95% Ar gas (Praxair) for one hour prior to each experiment. All experiments were conducted in a 0.1 $mol.l^{-1}$ NaCl (Fisher Scientific) + 0.05 $mol.l^{-1}$ $NaHCO_3/Na_2CO_3$ (EMD Chemicals) solution, with the pH adjusted to 9.5 using 0.5 $mol.l^{-1}$ NaOH. H_2O_2 was added by diluting a 3% W/V solution (Fisher Scientific).

[z]E-mail: jjnoel@uwo.ca

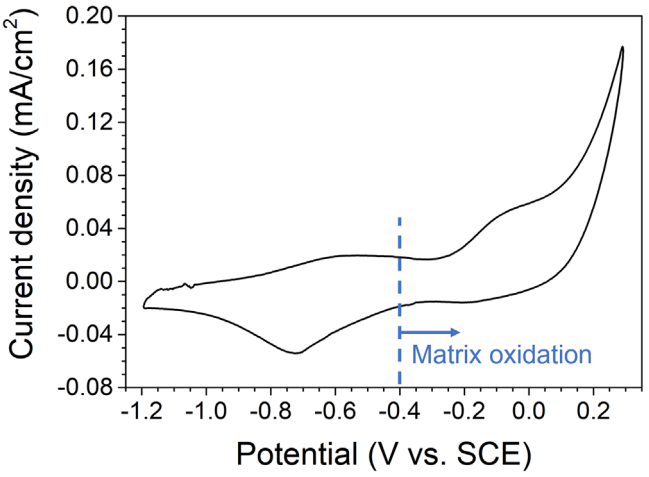

Figure 1. Cyclic voltammogram recorded on a UO_2 electrode in Ar-purged 0.1 mol.l^{-1} NaCl + 0.05 mol.l^{-1} HCO_3^-/CO_3^{2-} solution adjusted to pH 9.5. The vertical dashed line at ∼−400 mV (vs SCE) indicates the thermodynamic threshold for matrix oxidation.

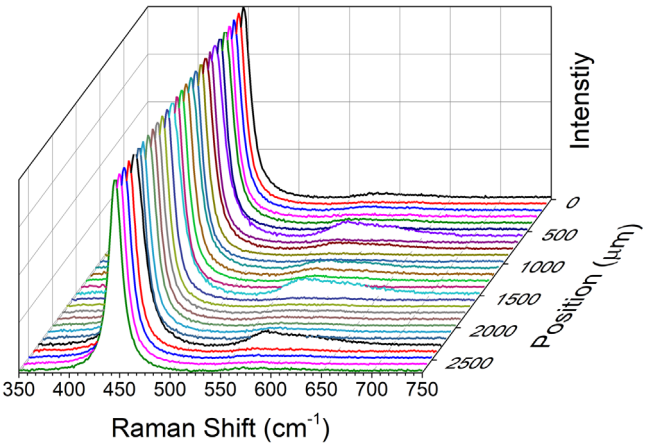

Figure 2. Raman spectra recorded across the surface of an unoxidized UO_2 specimen.

Electrochemical cell and equipment.—All experiments were conducted using a conventional 1 L three-electrode, three-compartment electrochemical cell. All potential measurements were recorded against a commercial saturated calomel electrode (SCE; 0.241 V vs standard hydrogen electrode).[46] A 1 cm^2 Pt foil spot-welded to a platinum wire was used as the counter electrode. The electrochemical cell was housed in a grounded Faraday cage to minimize interference from external electrical noise. Applied potentials and measured current responses were controlled, recorded, and analyzed using a Solartron Model 1480 Multistat and CorrWare software (Scribner Associates), respectively.

Electrochemical techniques.—Prior to each experiment, the UO_2 specimen was potentiostatically polarized to −1200 mV (vs SCE) for 2 min. This process removes any air-formed oxides on the surface to ensure that each experiment begins with a fresh surface.

Cyclic voltammetry (CV) experiments were performed to confirm the electrochemical viability of the UO_2 specimen. A potential scan was performed from −1200 mV (vs SCE) to a positive limit of 250 mV (vs SCE) and back at a scan rate of 10 mV.s^{-1}. The current interrupt method was used to compensate for electrode resistance.

Open circuit potential measurements were performed in solutions sparged with either UHP Ar (Praxair) or UHP 5% H_2/95% Ar (Praxair) (dissolved [H_2] ∼10^{-4} M). After reducing the surface electrochemically at −1200 mV (vs SCE) for 2 min, we allowed E_{CORR} to stabilize for 1–2 d before H_2O_2 additions.

Potentiostatic polarization (PSP) experiments were performed with UHP 5% H_2/95% Ar. After 1 d, to allow the system to reach a steady state, the UO_2 electrode was polarized to 0.1 V (vs SCE) or −0.1 V (vs SCE), with E_{CORR} being monitored both before and after polarization.

X-ray photoelectron spectroscopy.—X-ray photoelectron spectroscopy (XPS) was used to measure the surface composition of the electrode on completion of some experiments. Samples were transferred between the electrochemical cell and XPS instrument using a vacuum-sealed desiccator. Analyses were performed using a Kratos AXIS Supra Spectrometer with a monochromatic Al Kα (15 mA, 14 kV) radiation source (hν = 1486.6 eV). The instrument work function was calibrated for the Au 4f$_{7/2}$ metallic gold binding energy of 83.96 ± 0.025 eV, and the spectrometer dispersion was adjusted to a binding energy (BE) of 932.62 ± 0.025 eV for metallic Cu 2p$_{3/2}$. When necessary, surface charging was corrected by setting the C 1s BE at 284.8 eV. Survey spectra were collected over a BE range from 0 to 1100 eV, at a pass energy of 160 eV. High-resolution spectra were collected for O 1s, U 4 f, and C 1s at a pass energy of 20 eV. For all measurements, the area of analysis was ∼400 × 700 μm. All spectra were analyzed using CasaXPS software (version 2.3.19) with the fitting parameters used described elsewhere.[47]

Raman analyses.—Raman spectra were acquired using a Renishaw 2000 confocal Raman spectrometer (Renishaw, UK). Spectra were excited using a 50 mW He–Ne laser with a wavelength of 632.8 nm. The power of the laser beam was reduced to 50% to avoid heating effects. Spectra were recorded over the wavenumber range 150 to 1400 cm^{-1}. A Gaussian-Lorentzian peak model with a Shirley background correction was used to fit spectra. The deconvolution of the broad band between 500 and 700 cm^{-1} was performed as previously described.[48,49]

Results and Discussion

Figure 1 shows a CV recorded from −1200 mV (vs SCE) to +250 mV (vs SCE), with the vertical line at ∼−400 mV (vs SCE) indicating the thermodynamic threshold for oxidation of stoichiometric UO_2. By confining the negative potential limit to −1200 mV (vs SCE), the possibility of reducing any oxidized states (U^V) pre-existing in the UO_2 specimen was avoided, as demonstrated previously.[45] Consequently, the shallow, sub-thermodynamic oxidation current observed on the forward scan (from ∼−800 mV to −400 mV) can be attributed to the oxidation of pre-existing non-stoichiometric locations within the UO_2 matrix. This sub-thermodynamic oxidation at such sites is thought to be associated with grain boundaries,[50,51] and has been observed previously and characterized in detail.[44,50,52,53] The current plateau observed when the scan was extended to more positive potentials can be attributed to the anodic oxidation of the surface of the $U^{IV}O_2$ matrix to a thin layer (a few nm) of $U^{IV}_{1-2x}U^{V}_{2x}O_{2+x}$. The final rise in current, as the positive potential limit was approached, is attributable to the further oxidation of this layer to soluble uranyl carbonate complexes $(U^{VI}O_2(CO_3)_x)^{(2-2x)+}$.[53] The cathodic peak observed on the reverse scan has been shown to be due to the partial reduction of the surface layer.[53]

A series of Raman spectroscopic spot analyses yielded mainly spectra exhibiting only a single peak located at 445 cm^{-1}, assigned to the symmetric O-U^{IV} stretching mode in an undisturbed stoichiometric lattice. However, a number of locations exhibited both this peak and a broad shallow band located between 500 and 700 cm^{-1}, Fig. 2, indicative of a disturbed lattice. Deconvolution of this band yielded a peak at 575 cm^{-1}, assigned to a first-order LO phonon, and a second peak at 630 cm^{-1}.[48] This latterpeak can be attributed to distortion of the anion sublattice involving the formation of clusters of interstitial O atoms and is a signature of a degree of non-stoichiometry consistent with the voltammetric observation, Fig. 1.[54,55]

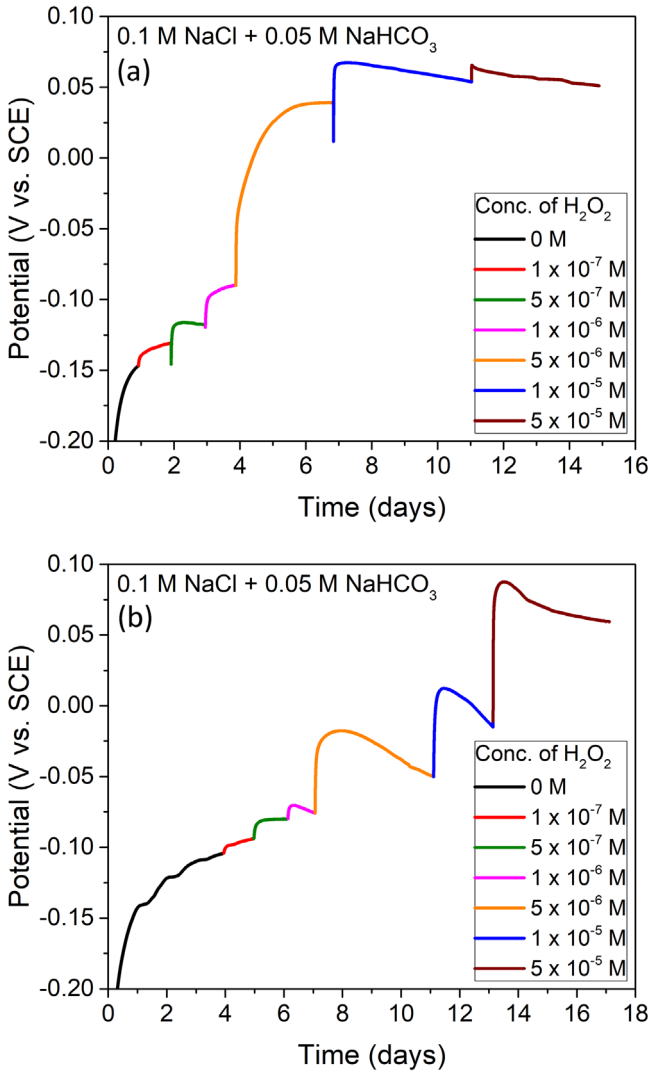

Figure 3. E_{CORR} as a function of time with sequential additions of $[H_2O_2]$, recorded on a natural UO_2 electrode in 0.1 mol.l^{-1} NaCl + 0.05 mol.l^{-1} HCO_3^-/CO_3^{2-} solution adjusted to pH 9.5 with (a) Ar, or (b) 5% H_2/95% Ar sparge gas. The legend values show the actual concentration of H_2O_2 during that measurement period.

Figure 3 shows a series of E_{CORR} measurements in solutions sparged with either Ar (Fig. 3a or 5% H_2/95% Ar (Fig. 3b). Prior to the first H_2O_2 addition, E_{CORR} was allowed to approach a steady state. Irrespective of the sparge gas, E_{CORR} increased to a value between −150 mV (vs SCE) and −100 mV (vs SCE). Since the thermodynamic threshold for the oxidation of stoichiometric UO_2 is ∼−400 mV (vs SCE) for the conditions employed in these experiments, Fig. 1, these values suggest a slight oxidation of the UO_2 surface, probably by traces of dissolved O_2.

In the absence of H_2, Fig. 3a, each H_2O_2 addition led to a small increase in E_{CORR} to a new steady-state value, up to $[H_2O_2] = 10^{-6}$ M. For $[H_2O_2] = 5 \times 10^{-6}$ M, a very marked increase in E_{CORR} occurred, with subsequent increases in $[H_2O_2]$ leading to only minor further increases and the potential stabilizing around ∼60 mV (vs SCE). When H_2 was present (in the present case at $\sim 10^{-4}$ M), Fig. 3b, increases in $[H_2O_2]$ up to 10^{-6} M led to similar small increases in E_{CORR}. However, when $[H_2O_2]$ was increased to $>10^{-6}$ M, a rapid initial increase in E_{CORR} was eventually reversed. A similar initial increase/subsequent decrease was observed for $[H_2O_2] = 10^{-5}$ M. However, at 5×10^{-5} M, the eventual decrease was arrested, as E_{CORR} decreased only slightly and approached a steady-state value of ∼60 mV (vs SCE). This indicates an insensitivity to H_2 for $[H_2O_2] \geqslant 5 \times 10^{-5}$ M on the time scale of this experiment. Similar E_{CORR} behaviour has been consistently observed on SIMFUELs containing rare Earth dopants and ε-particles or rare Earth dopants only.[22,29] While the general form of the transients (in the absence and presence of H_2) is reproducible, the actual values recorded can vary as observed in this study and previously.

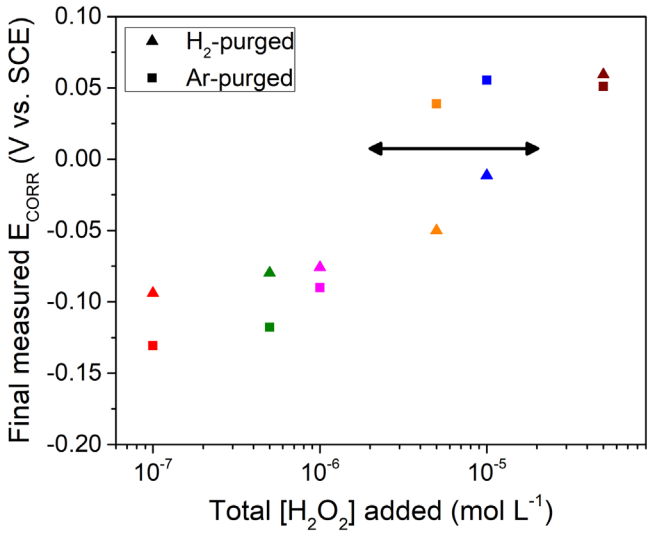

Figure 4. Final E_{CORR} values from Fig. 3, as a function of total $[H_2O_2]$. The horizontal arrow indicates the range in which E_{CORR} is sensitive to the presence of H_2.

Figure 4 shows the final measured values of E_{CORR}, from Fig. 3, as a function of the total $[H_2O_2]$ in the solution. While the values for $[H_2O_2] < 10^{-6}$ M may reflect the influence of traces of dissolved O_2, which could be present at a concentration ⩾ that of the added H_2O_2, there is a clear separation in the values measured in the presence and absence of H_2 in the $[H_2O_2]$ range indicated approximately by the horizontal arrow. At the highest $[H_2O_2]$ (5×10^{-5} M), there is no difference in the two values, indicating an insensitivity to H_2 in this range. This clearly demonstrates that H_2 (at a concentration of $\sim 10^{-4}$ M) can interfere with the reactions of H_2O_2 on the UO_2 surface when $[H_2O_2]$ is in the concentration range between approximately 10^{-6} M and 10^{-5} M. It is likely that this interference extends to lower $[H_2O_2]$ but is undetectable in these measurements.

A similar insensitivity of E_{CORR} to $[H_2O_2] \geqslant 10^{-5}$ M has been observed previously on undoped UO_2 and attributed to the redox buffering of the H_2O_2 decomposition reaction. Under these conditions, the equilibrium potentials for the two half-reactions involved, reactions 1 and 2, exhibit dependencies on $[H_2O_2]$ which are identical but opposite in sign. Providing both reactions are rapid and equally influenced by $[H_2O_2]$, a change in $[H_2O_2]$ would change the decomposition rate without influencing E_{CORR}.

$$H_2O_2 + 2e^- \rightarrow 2OH^- \quad [1]$$

$$H_2O_2 \rightarrow O_2 + 2H^+ + 2e^- \quad [2]$$

The decomposition of H_2O_2 proceeds on the surface of various metal oxides via a radical mechanism.[32–38]

$$(H_2O_2)_{ads} \rightarrow 2(OH^\bullet)_{ads} \quad [3]$$

$$(H_2O_2)_{ads} + (OH^\bullet)_{ads} \rightarrow H_2O + (HO_2^\bullet)_{ads} \quad [4]$$

$$2(HO_2^\bullet)_{ads} \rightarrow H_2O_2 + O_2 \quad [5]$$

On UO_2, this process has been shown to be catalyzed by the presence of a thin $U^{IV}_{1-2x}U^{V}_{2x}O_{2+x}$ surface layer; i.e., by the

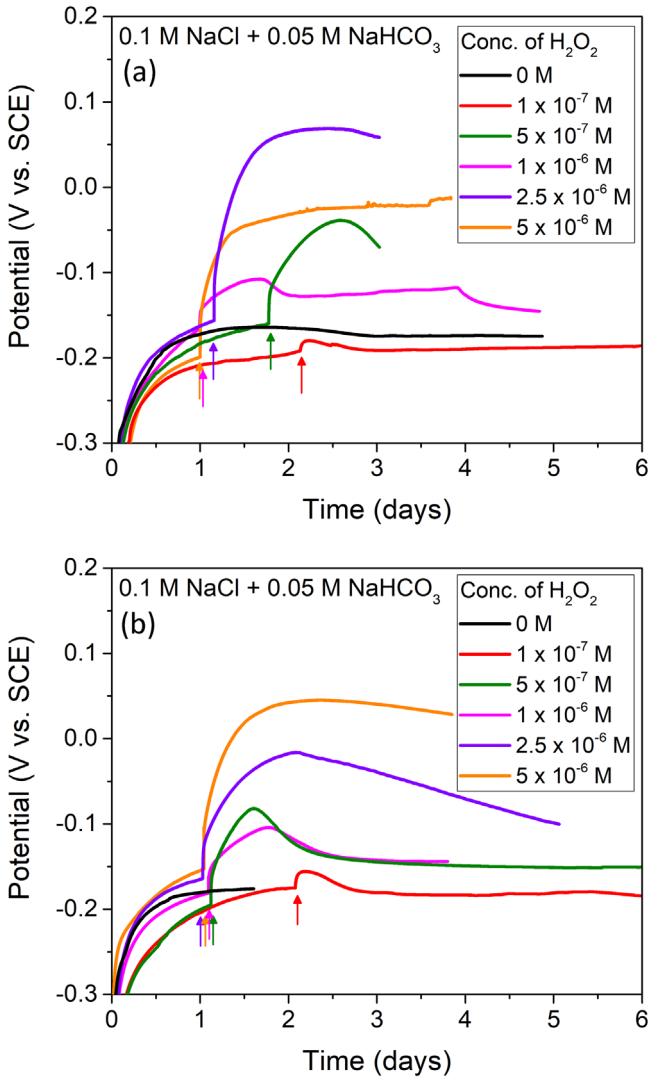

Figure 5. E_{CORR} as a function of time, before and after individual additions of H_2O_2 (indicated by arrows), prior to XPS analyses. The sparge gas was either (a) Ar or (b) 5% H_2/95% Ar.

formation and destruction of U^V surface sites accompanied by the incorporation and release of O^{2-} at vacant interstitial sites readily available in the UO_2 cubic lattice.[56] This peroxide decomposition process occurs in competition with the oxidative dissolution (corrosion) of the UO_2 surface via the extraction of the U^V state (from the $U^{IV}_{1-2x}U^V_{2x}O_{2+x}$ surface layer) and its further oxidation to U^{VI} and release to solution as a HCO_3^-/CO_3^{2-} -complexed uranyl ion[13]

$$U^V(\text{in } U^{IV}_{1-2x}U^V_{2x}O_{2+x}) + HCO_3^- \rightarrow (U^VO_2HCO_3)_{ads} + e^- \quad [6]$$

$$(U^VO_2HCO_3)_{ads} + OH^- \rightarrow (U^{VI}O_2CO_3)_{ads} + H_2O + e^- \quad [7]$$

$$(U^{VI}O_2CO_3)_{ads} + (y-1)HCO_3^- \rightarrow U^{VI}O_2(CO_3)_y^{(2-2y)+} + (y-1)H^+ \quad [8]$$

with the electrons consumed by the reduction of $(OH^\bullet)_{ads}$.

$$2(OH^\bullet)_{ads} + 2e^- \rightarrow 2OH \quad [9]$$

The balance between H_2O_2 decomposition and UO_2 dissolution depends not only on the $[H_2O_2]$ and $[CO_3]_{tot}$ ($[HCO_3^-] + [CO_3^{2-}]$) but also on the composition of the $U^{IV}_{1-2x}U^V_{2x}O_{2+x}$ surface layer. It also depends on whether or not the oxide matrix is stabilized by rare Earth (RE^{III}) doping, with ~14% of the H_2O_2 consumed by dissolution on undoped UO_2 but <4% on RE^{III}-doped UO_2.[56,57]

It should be noted that Cl^- and HCO_3^-/CO_3^{2-} ions in solution can also react with hydroxyl radicals on the UO_2 surface.[58] However, all solutions used for immersion experiments had constant [NaCl] and [$NaHCO_3/Na_2CO_3$], resulting in a consistent influence on the surface reactions. The effect of these ions is therefore not considered in this article.

Figure 5 shows a series of individual E_{CORR} measurements at different single $[H_2O_2]$ values. As observed in Fig. 3, E_{CORR} increased, prior to the addition of H_2O_2 in both the absence (Fig. 5a) and presence (Fig. 5b) of H_2, towards a steady-state value between −160 mV (vs SCE) and −200 mV (vs SCE). The increases are attributed to slight surface oxidation due to trace dissolved O_2. This occurred independently of the presence of H_2, confirming there is no detectable influence of H_2 in the absence of H_2O_2. The values recorded after H_2O_2 addition did not show the same consistent behaviour as in the first set of experiments (Fig. 3). However, the tendency to more readily generate a peak in the presence of H_2 was

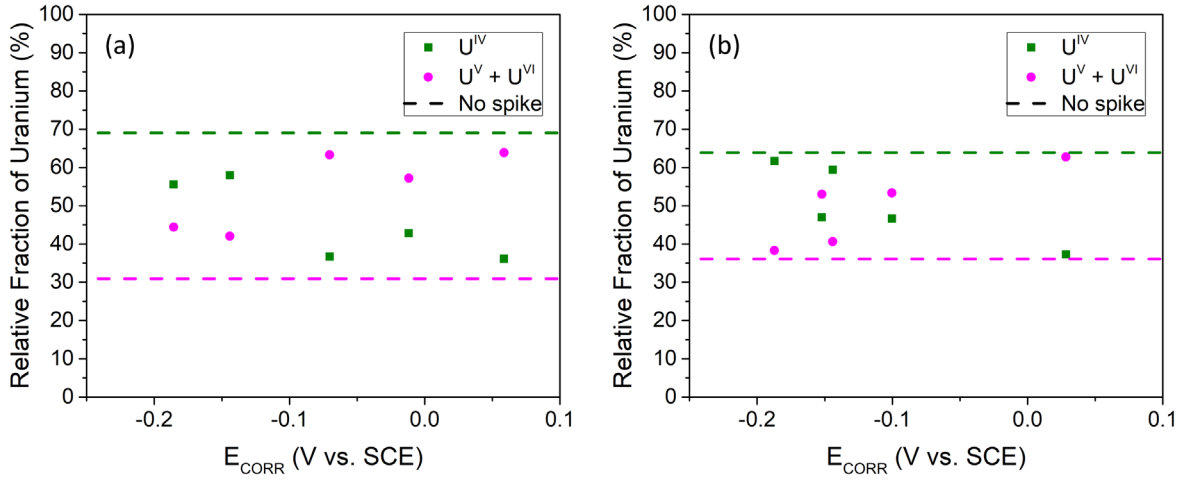

Figure 6. Surface compositions recorded on a natural UO_2 electrode as a function of the final measured E_{CORR} in a solution sparged with either (a) Ar or (b) 5% H_2/95% Ar (from Fig. 5). The horizontal dashed lines refer to the percentages of U^{IV} (green) and $U^V + U^{VI}$ (magenta) after experiments with no H_2O_2 added.

observed. As discussed below, this is not surprising given the competition between surface oxidation and oxidant scavenging in the presence of surface radical species. While the results collected in this study were based on single experiments, the behaviour observed (with and without H_2) was consistent with our previous observations.[22,29]

After the individual H_2O_2 addition experiments, the extent of surface oxidation was determined by XPS, Fig. 6. The percentages of reduced (U^{IV}) and oxidized (U^{V} and U^{VI}) states are plotted as a function of the final E_{CORR} value recorded. Although the individual fractions of U^{V} and U^{VI} are determined when deconvoluting the XPS spectra, as described elsewhere,[29] the extent of air oxidation from U^{V} to U^{VI} is difficult to control, making the relative analyzed contributions of U^{V} and U^{VI} somewhat variable. This makes the sum of the two states ($U^{V} + U^{VI}$) a more reliable indication of the extent of oxidation.

Figure 6 shows that, despite the absence of a clear relationship between E_{CORR} and $[H_2O_2]$, Fig. 5, the surface composition is dependent on the final measured value of E_{CORR}. The data show that the extent of oxidation increases as E_{CORR} becomes more positive in both Ar and Ar/H_2 sparged solutions. A similar analysis of the oxidation state of the surface after each incremental addition of H_2O_2 (Fig. 3) was not possible. This introduces the possibility that the transient behaviour in E_{CORR} observed in these experiments when H_2 is present, Fig. 3b, can be attributed to a rapid initial oxidation of the surface when H_2O_2 is first added, followed by a subsequent reduction of the temporarily oxidized UO_2 surface. These results suggest that the anticipated scavenging of the surface $OH^{\bullet}$ radicals, created by reaction 3, by dissolved H_2 could involve catalysis by the U^{IV}/U^{V} states in the UO_2 surface.

$$U^{IV} + (OH^{\bullet})_{ads} \rightarrow U^{V} + OH^{-} \quad [10]$$

$$H_2 + (OH^{\bullet})_{ads} \rightarrow (H^{\bullet})_{ads} + H_2O \quad [11]$$

$$U^{V} + (H^{\bullet})_{ads} \rightarrow U^{IV} + H^{+} \quad [12]$$

The ability of $H^{\bullet}$ radicals to reduce U^{V} states in a UO_2 surface has been demonstrated in gamma radiolysis experiments.[45]

Figure 7 shows the relationship between the final measured E_{CORR} values (from Fig. 4) and the surface composition expressed as a fraction of surface oxidized states ($(U^{V} + U^{VI})/U_{tot}$). The amounts of surface oxidized states are compared to the composition of a Gd-doped UO_2 surface after electrochemical treatment at a series of applied potentials for 1 h in a solution with the same composition as that used in the experiments in this paper.[45,49] The increase in oxidized surface states with potential was considerably steeper for the undoped UO_2 from this study than that observed on the Gd-doped UO_2. The enhanced stability of RE^{III}-doped UO_2 against oxidation has been shown to be due to the formation of RE^{III}-oxygen vacancy (O_V) clusters. These clusters limit the available number of O_V, which are required to accommodate interstitial oxygen (O_i) ions as UO_2 is oxidized to $U^{IV}_{1-2x}U^{V}_{2x}O_{2+x}$.[49]

Several regions (A to D) are noted in Fig. 7, in addition to several compositions for specific fractions of oxidized surface states. These regions denote specific ranges of composition and lattice structure determined by He and Shoesmith using Raman spectroscopy.[48] For relatively low degrees of non-stoichiometry (region A), excess oxygen is randomly distributed within the oxidized surface, with an increase in the value of x (in $U^{IV}_{1-2x}U^{V}_{2x}O_{2+x}$) leading to the association of O_i ions into clusters. For a sufficiently high degree of non-stoichiometry ($x \geqslant 0.15$) (region B), the generation of large cuboctahedral clusters leads to a significant loss of cubic symmetry, resulting in the onset of a cubic to tetragonal structural transition and the initiation of dissolution.[53] In region C, the UO_2 achieves a terminal irreversible composition for the fluorite structure ($U^{IV}_{0.34}U^{V}_{0.66}O_{2.33}$). Region D, indicated by the horizontal arrow, shows the potential range (and, hence, the range of surface compositions) over which the sequence of reactions 10 to 12 can be sustained, allowing H_2 to scavenge $OH^{\bullet}$ radicals and possibly control the surface composition. It is likely that H_2 scavenging of $OH^{\bullet}$ radicals and, hence, a suppression of surface oxidation, the first essential step in the dissolution process (reactions 6 to 8), is possible at lower $[H_2O_2]$ (and, hence, lower E_{CORR}) but is not detectable in these experiments. Although the potential region over which $(H^{\bullet})_{ads}$ species appear able to suppress or reverse surface oxidation is narrow (region D) and the change in composition is significant, leading to some uncertainty, these results suggest an ability of the $U^{IV}_{1-2x}U^{V}_{2x}O_{2+x}$ layer to act catalytically via the reaction sequence 10 to 12. Once the surface reaches the terminal composition (region E), $OH^{\bullet}$ radical scavenging is kinetically more difficult, as indicated by the only minor reversibility of E_{CORR} when $[H_2O_2] \geqslant 10^{-5}$ M (Fig. 3). At sufficiently high $[H_2O_2]$ and E_{CORR}, within region E, the dominant reaction is H_2O_2 decomposition (reactions 3 to 5) accompanied by some dissolution (reactions 6 to 8). Whether or not $OH^{\bullet}$ radical scavenging would compete with these reactions at higher $[H_2]$ remains to be investigated.

To demonstrate that H_2 is only active on the surface at compositions less oxidized than the terminal composition

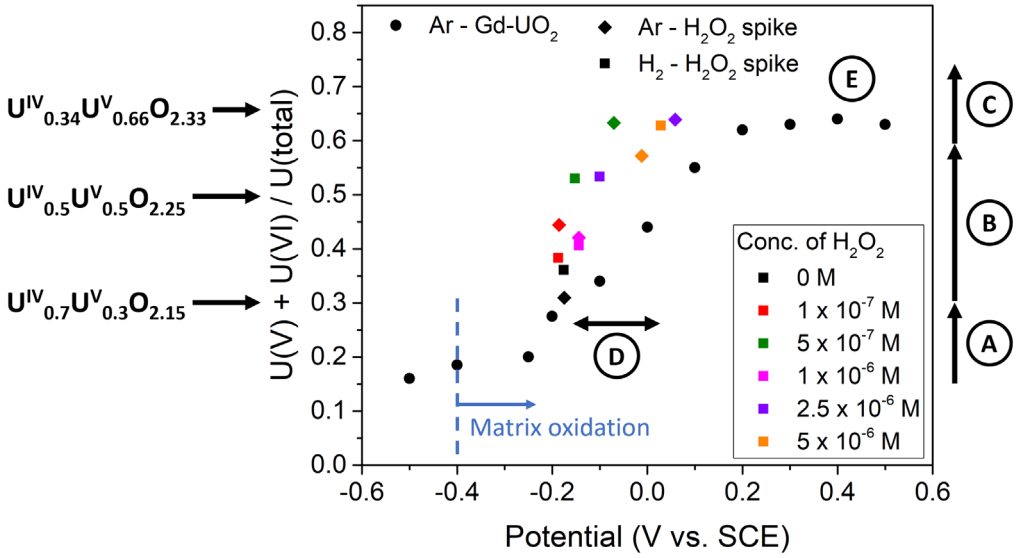

Figure 7. Comparison of $(U^{V} + U^{VI})/U_{total}$ ratios at different $[H_2O_2]$ as a function of potential. The solid circles were measured on a Gd-UO_2 electrode in Ar-sparged 0.1 mol.l^{-1} NaCl + 0.05 mol.l^{-1} HCO_3^{-}/CO_3^{2-} solution.[60]

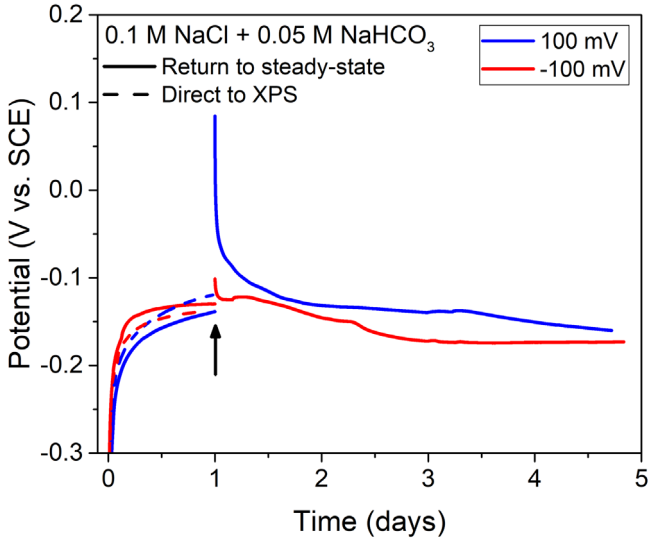

Figure 8. E_{CORR} as a function of time in a solution sparged with 5% H_2/95% Ar. The arrow indicates the time at which the electrode was potentiostatically polarized to either 100 mV (blue) or −100 mV (red). XPS was performed immediately after polarization (dashed) or after 4 d of allowing the system to return to a steady state (solid).

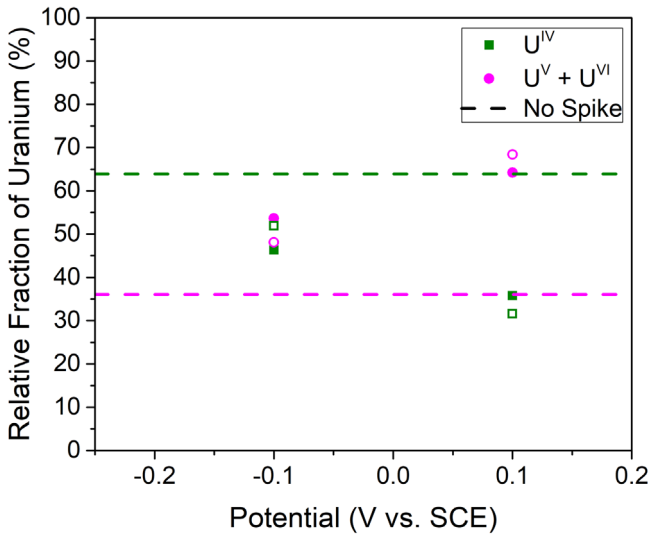

Figure 9. Surface compositions recorded as a function of the polarization potential from Fig. 8. XPS was performed immediately after polarization (open points) or after 4 d of allowing the system to return to a steady state (solid points). The horizontal dashed lines refer to the percentages of U^{IV} (green) and $U^{V} + U^{VI}$ (magenta) after experiments with no H_2O_2 added.

$(U^{IV}_{0.34}U^{V}_{0.66}O_{2.33})$ in the presence of $OH^{\bullet}$ radicals, a set of potentiostatic polarization experiments were performed in a H_2-sparged solution. After reaching a steady state E_{CORR}, the electrode was electrochemically oxidized at −100 mV (vs SCE) or 100 mV (vs SCE) for one hour and immediately analyzed by XPS. In an additional experiment, the electrode was electrochemically oxidized, then E_{CORR} was measured for 4 d before XPS analysis was repeated. The E_{CORR}-time curves and the oxidized fractions $((U^{V} + U^{VI})/U_{tot})$ are shown in Figs. 8 and 9, respectively. Despite the applied overpotential, E_{CORR} rapidly recovered to steady-state values measured prior to polarization. For both applied overpotentials, there was little difference between the surface compositions recorded immediately after polarization and after 4 d at E_{CORR}. This is unsurprising for the −100 mV overpotential, as the steady state E_{CORR} is only slightly lower than the applied overpotential. In

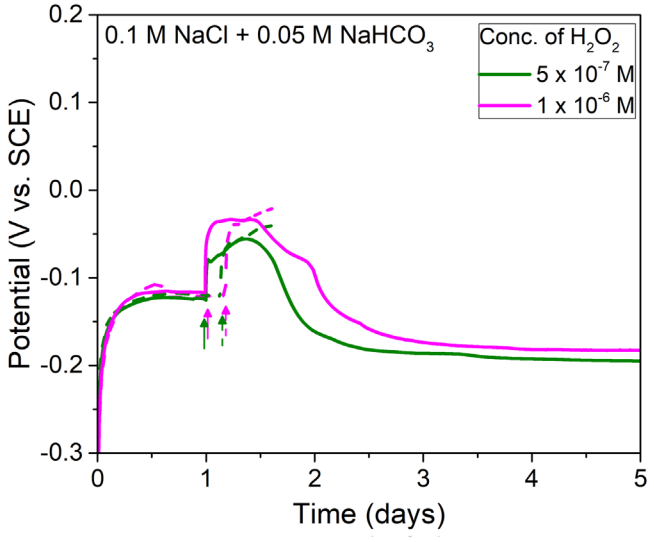

Figure 10. E_{CORR} as a function of time in a solution sparged with 5% H_2/95% Ar. The arrows indicate the times at which H_2O_2 was added. Electrodes were removed for XPS analysis at either the peak potential (dashed lines) or after the eventual achievement of a steady state (solid lines).

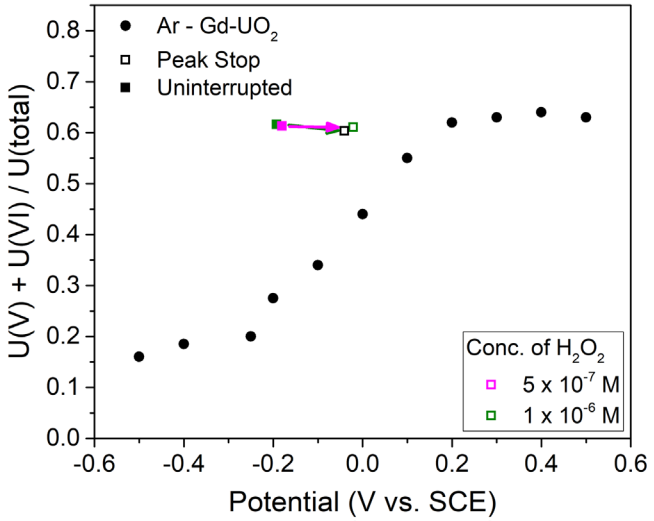

Figure 11. Comparison of $(U^{V} + U^{VI})/U_{total}$ ratio as a function of potential. XPS analysis was performed after the immersion experiment (Fig. 10) at peak potential (open points) or after the potential returned to a steady state (solid points).

comparison with to Fig. 7, the compositions are in reasonable agreement. However, even though E_{CORR} rapidly recovered to those values measured prior to applying the 100 mV overpotential, the surface composition remained close to the terminal composition $(U^{IV}_{0.34}U^{V}_{0.66}O_{2.33})$. While $U^{VI}O_2^{2+}$ formed at this potential would be expected to dissolve as $U^{VI}O_2(CO_3)_y^{(2-2y)+}$ via reaction 8, this result demonstrates that H_2 alone cannot reduce the extensively oxidized surface on the time scale of this experiment.

To further investigate the ability of H_2 to reduce a partially oxidized UO_2 surface in H_2O_2 containing solutions, experiments from Fig. 5 were repeated for $[H_2O_2]$ of 5×10^{-7} M and 10^{-6} M under a H_2 sparged environment. In all experiments, the system was left for 24 h to establish a steady-state E_{CORR} before the qddition of H_2O_2, indicated by the vertical arrows. After the H_2O_2 was added, either the system was left to return to a steady state (solid line) or the experiment was terminated before E_{CORR} could begin to recover from the initial increase (dashed line), Fig. 10.

Following each experiment, the sample was taken for XPS analysis to determine the fraction of surface oxidized states, Fig. 11. The reproducibility of the initial increase in E_{CORR} allowed for reliable termination at the maximum E_{CORR} value of ~ -50 mV (vs SCE). When left to return to a steady state, E_{CORR} decreased to a value lower than the pre-addition value. The surface oxidation ratio for all experiments was approximately 0.66, regardless of the initial $[H_2O_2]$ or final measured E_{CORR}. While H_2 was shown to reduce the UO_2 surface over the same concentration range in previous experiments, Fig. 7, this was not observed in the current experiments. This confirms that once the UO_2 surface reaches the terminal composition of $U^{IV}_{0.34}U^{V}_{0.66}O_{2.33}$, the formation of cuboctahedral defect clusters occurs.[53] When such lattice defects form, H_2 is unable to reduce the surface regardless of the presence of H_2O_2 or the value of E_{CORR}. The transient observed in E_{CORR} is therefore more likely to have been due to the continued consumption of H_2O_2 rather than the reduction of the UO_2 surface.

Summary and Conclusions

Based on these results, it can be claimed that H_2 can scavenge $(OH^{\bullet})_{ads}$, which would otherwise oxidize the UO_2 surface, catalyze the decomposition of H_2O_2, and stimulate a small amount of dissolution. These results are consistent with recently published model predictions.[59] Whether or not the H_2, as $(H^{\bullet})_{ads}$, is involved in changing the surface composition is not clear.

The results in Figs. 7 and 11 suggest that H_2 may reduce U^{V} states on the surface, providing the extent of surface oxidation by $(OH^{\bullet})_{ads}$ is limited, and the value of x in $U^{IV}_{1-2x}U^{V}_{2x}O_{2+x}$ remains <0.25; i.e., within the composition range where O_i remain randomly distributed, allowing surface oxidation to be reversed. At higher values of x, when O_i are dominantly located within defect clusters, reversibility of the surface composition does not appear to occur, and H_2O_2 decomposition is the dominant reaction. Whether $(H^{\bullet})_{ads}$ produced by the scavenging of $(OH^{\bullet})_{ads}$ have an influence in re-reducing the $U^{IV}_{1-2x}U^{V}_{2x}O_{2+x}$ surface layer remains to be demonstrated. This is likely to require experiments at higher H_2 concentrations.

Acknowledgments

This work was jointly funded by the Natural Sciences and Engineering Research Council of Canada and the Nuclear Waste Management Organization through Alliance Grant ALLRP561193-20. Surface Science Western is acknowledged for the use of their instruments.

ORCID

Martin D. M. Badley https://orcid.org/0009-0006-9267-1312
James J. Noël https://orcid.org/0000-0003-3467-4778

References

1. D. S. Hall, M. Behazin, W. J. Binns, and P. G. Keech, *Prog. Mater Sci.*, **118**, 100766 (2021).
2. L. Werme and C. Lilja, *Fuel and canister process report for the safety assessment SR-Site, SKB TR-10-46*, Swedish Nuclear Fuel and Waste Management Co., Stockholm, Sweden (2010).
3. L. H. Johnson and D. W. Shoesmith, "Spent fuel." *in Radioactive Waste Forms for the Future*, ed. W. B. Lutze and R. C. Ewing (Elsevier, Amsterdam, Netherlands) 20, 635 (1988).
4. L. H. Johnson, D. M. LeNeveu, D. W. Shoesmith, D. W. Oscarson, M. N. Gray, R. J. Lemire, and N. C. Garisto, *The disposal of Canada's nuclear fuel waste: the vault model for postclosure assessment*, Atomic Energy of Canada Ltd., Canada (1994).
5. D. W. Shoesmith, J. C. Tait, S. Sunder, W. J. Gray, S. A. Steward, R. E. Russo, and J. D. Rudnicki, *Factors affecting the differences in reactivity and dissolution rates between UO_2 and spent nuclear fuel, AECL-11515*, Atomic Energy of Canada Ltd., Canada (1995).
6. B. Grambow, A. Loida, P. Dressler, H. Geckeis, J. Gago, I. Casas, J. D. Pablo, J. Gimenez, and M. E. Torrero, *Long-term safety of radioactive waste disposal: Chemical reaction of fabricated and high burnup spent UO_2 fuel with saline brines Final report*, Forschungszentrum Karlsruhe, Germany (1996).
7. B. Grambow et al., *NF-PRO RTD Component 1: Dissolution and release from the waste matrix, EUR 23730*, European Commission, Brussels (2008), Brussels.
8. B. Grambow et al., *Model uncertainty for the mechanism of dissolution of spent fuel in a nuclear waste repository, EUR 24597 EN*, European Commission, Brussels (2010).
9. C. Poinssot, C. Ferry, M. Kelm, B. Grambow, A. Martinez-Esparza, L. Johnson, Z. Andriambololona, J. Bruno, C. Cachoir, and J. M. Cavendon, *Final report of the European project spent fuel stability under repository conditions*, Atomic Energy Commission (CEA), Gif-sur-Yvette, France (2005).
10. V. M. Oversby, *Rates and mechanisms of radioactive release and retention inside a waste disposal canister - in Can Processes NEI-SE-562*, Swedish Nuclear Fuel and Waste Management Co., Stockholm, Sweden (2003).
11. B. Kienzler, V. Metz, and A. Valls, *FIRST-Nuclides: Fast/Instant release of safety relevant radionuclides from spent nuclear fuel FP7-295722; Deliverable 5.13*, European Commission, EURATOM FP7 Collaborative Project, Luxembourg, Germany (2015).
12. K. Lemmens, C. Cachoir, and T. Mennecart, *Dissolution behaviour of spent nuclear fuel at highly alkaline conditions 27622175, ER-0505*, SCK CEN, Belgium (2019).
13. M. Badley and D. W. Shoesmith, *The corrosion/dissolution of used nuclear fuel in a deep geologic repository NWMO-TR–09*, Nuclear Waste Management Organization, Toronto, Canada (2022).
14. I. Grenthe, J. Fuger, R. J. Konings, R. J. Lemire, A. B. Muller, C. Nguyen-Trung, and H. Wanner, *Chemical Thermodynamics of Uranium* (Elsevier, Amsterdam) (1992).
15. E. Ekeroth, O. Roth, and M. Jonsson, *J. Nucl. Mater.*, **355**, 38 (2006).
16. N. Z. Liu, L. D. Wu, Z. Qin, and D. W. Shoesmith, *Environ. Sci. Technol.*, **50**, 12348 (2016).
17. L. D. Wu, Z. Qin, and D. W. Shoesmith, *Corros. Sci.*, **84**, 85 (2014).
18. T. E. Eriksen, D. W. Shoesmith, and M. Jonsson, *J. Nucl. Mater.*, **420**, 409 (2012).
19. M. E. Broczkowski, D. Zagidulin, and D. W. Shoesmith, "The role of dissolved hydrogen on the corrosion/dissolution of spent nuclear fuel." *Nuclear Energy and the Environment*, ed. C. M. Wai and B. J. Mincher (Washington, DC)(American Chemical Society) Vol. 1046, Chap. 26, p. 349 (2010).
20. J. K. Nørskov, T. Bligaard, A. Logadottir, J. Kitchin, J. G. Chen, S. Pandelov, and U. Stimming, *J. Electrochem. Soc.*, **152**, J23 (2005).
21. J. C. Wren, D. W. Shoesmith, and S. Sunder, *J. Electrochem. Soc.*, **152**, B470 (2005).
22. M. E. Broczkowski, P. G. Keech, J. J. Noël, and D. W. Shoesmith, *J. Electrochem. Soc.*, **158**, C439 (2011).
23. M. E. Broczkowski, J. J. Noël, and D. W. Shoesmith, *J. Nucl. Mater.*, **346**, 16 (2005).
24. M. E. Broczkowski, P. G. Keech, J. J. Nol, and D. W. Shoesmith, *J. Electrochem. Soc.*, **157**, C275 (2010).
25. P. Carbol, J. Cobos-Sabate, J. P. Glatz, B. Grambow, B. Kienzler, A. Loida, A. Martinez Esparza Valiente, V. Metz, J. Quiñones, and C. Ronchi, *The effect of dissolved hydrogen on the dissolution of ^{233}U doped UO_2(s) high burn-up spent fuel and MOX fuel TR-05-09*, Swedish Nuclear Fuel and Waste Management Co., Stockholm, Sweden (2005).
26. T. Eriksen and M. Jonsson, *The effect of hydrogen on dissolution of spent fuel in 0.01 mol/dm^{-3} $NaHCO_3$ solution TR-07-06*, Swedish Nuclear Fuel and Waste Management Co., Stockholm, Sweden (2007).
27. D. W. Shoesmith, *The role of dissolved hydrogen on the corrosion/dissolution of spent nuclear fuel NWMO-TR–19*, Nuclear Waste Management Organization, Toronto, Canada (2008).
28. M. E. Broczkowski, J. J. Noël, and D. W. Shoesmith, *J. Electroanal. Chem.*, **602**, 8 (2007).
29. M. Razdan and D. W. Shoesmith, *Faraday Discuss.*, **180**, 283 (2015).
30. L. Bauhn, N. Hansson, C. Ekberg, P. Fors, and K. Spahiu, *J. Nucl. Mater.*, **507**, 38 (2018).
31. S. Nilsson and M. Jonsson, *J. Nucl. Mater.*, **372**, 160 (2008).
32. C. M. Lousada, M. Yang, K. Nilsson, and M. Jonsson, *J. Mol. Catal. A: Chem.*, **379**, 178 (2013).
33. A. Barreiro-Fidalgo, Y. Kumagai, and M. Jonsson, *J. Coord. Chem.*, **71**, 1799 (2018).
34. S.-S. Lin and M. D. Gurol, *Environ. Sci. Technol.*, **32**, 1417 (1998).
35. D. Fu, X. Zhang, P. G. Keech, D. W. Shoesmith, and J. C. Wren, *Electrochim. Acta*, **55**, 3787 (2010).
36. A. Hiroki and J. A. LaVerne, *J. Phys. Chem. B*, **109**, 3364 (2005).
37. D. Zigah, J. Rodríguez-López, and A. J. Bard, *Phys. Chem. Chem. Phys.*, **14**, 12764 (2012).
38. C. M. Lousada, M. Trummer, and M. Jonsson, *J. Nucl. Mater.*, **434**, 434 (2013).
39. M. Razdan, *Electrochemical and Surface Compositional Studies on Uranium Dioxide (PhD dissertation)*, University of Western Ontario, London, Ontario (2013).
40. N. Dudney, R. Coble, and H. Tuller, *J. Am. Ceram. Soc.*, **64**, 627 (1981).
41. L. Collier, R. Hampton, G. Saunders, and A. Stoneham, *J. Nucl. Mater.*, **168**, 268 (1989).
42. G. J. Hyland and J. Ralph, *High Temp-High Pressures*, **15**, 179 (1983).
43. P. Winter, *J. Nucl. Mater.*, **161**, 38 (1989).
44. H. He, R. K. Zhu, Z. Qin, P. Keech, Z. Ding, and D. W. Shoesmith, *J. Electrochem. Soc.*, **156**, C87 (2009).

45. N. Liu, F. King, J. J. Noël, and D. W. Shoesmith, *Corros. Sci.*, **192**, 109776 (2021).
46. C. G. Zoski, *Handbook of Electrochemistry* (Elsevier, Amsterdam) (2006).
47. M. Razdan, D. S. Hall, P. G. Keech, and D. W. Shoesmith, *Electrochim. Acta*, **83**, 410 (2012).
48. H. He and D. W. Shoesmith, *Phys. Chem. Chem. Phys.*, **12**, 8109 (2010).
49. M. Razdan and D. W. Shoesmith, *J. Electrochem. Soc.*, **161**, H105 (2014).
50. D. W. Shoesmith, *J. Nucl. Mater.*, **282**, 1 (2000).
51. T. Livneh and E. Sterer, *Phys. Rev. B: Condens. Matter*, **73**, 085118 (2006).
52. H. He, Z. Qin, and D. W. Shoesmith, *Electrochim. Acta*, **56**, 53 (2010).
53. N. Liu, H. He, J. J. Noël, and D. W. Shoesmith, *Electrochim. Acta*, **235**, 654 (2017).
54. J. M. Elorrieta, L. J. Bonales, N. Rodríguez-Villagra, V. G. Baonza, and J. Cobos, *Phys. Chem. Chem. Phys.*, **18**, 28209 (2016).
55. L. Desgranges, G. Baldinozzi, P. Simon, G. Guimbretière, and A. Canizares, *J. Raman Spectrosc.*, **43**, 455 (2012).
56. Z. Zhu, J. J. Noël, and D. W. Shoesmith, *Electrochim. Acta*, **340**, 135980 (2020).
57. S. Nilsson and M. Jonsson, *J. Nucl. Mater.*, **410**, 89 (2011).
58. D. E. Richardson, H. Yao, K. M. Frank, and D. A. Bennett, *J. Am. Chem. Soc.*, **122**, 1729 (2000).
59. N. L. Hansson and M. Jonsson, *Radiat. Phys. Chem.*, **210**, 111055 (2023).
60. M. Razdan and D. W. Shoesmith, *J. Electrochem. Soc.*, **161**, H225 (2014).